A new method to restore tectonically beheaded valleys

Adrien Moulin[1], Matthieu Ribot[1], Sigurjón Jónsson[1]

[1]King Abdullah University of Science and Technology (KAUST), Thuwal, Saudi Arabia

KEY POINTS

A new method is developed to restore tectonically beheaded drainages using chi-elevation distribution

The method is successfully applied to the Wadi-al-Akhdar Graben, Saudi Arabia

ABSTRACT

Tectonically beheaded valleys represent strain markers that can be used to constrain the geometry and kinematics of dip-slip faults. Quantifying the cumulative deformation they have recorded requires introducing several assumptions that are difficult to test, which limits their practical utility. Here we present a new method which eliminates some of these assumptions by focusing on pairs of beheaded valleys and analyzing them in the χ (horizontal channel coordinate normalized by drainage area) – elevation space. This approach allows tectonic deformation to be retrieved without using any information from the lost upstream catchment, and has therefore the potential of reducing uncertainties associated to the tectonic reconstruction of beheaded valleys. We demonstrate the power of this method by applying it to an outstanding beheaded stream network preserved across the Wadi-al-Akhdar Graben (NW Saudi Arabia). This methodological contribution is expected to revive the use of beheaded valleys by morpho-tectonic studies, and stimulate the exploration of its potential for long-term tectonic reconstructions

1. INTRODUCTION

Drainage capture and beheading represent extreme cases of divide mobility, during which large fractions of drainage areas are gained or lost suddenly. These events occur in both tectonically active and inactive environments as drainage networks evolve towards stable topologies (Bonnet et al., 2009 ; Giachetta and Willett, 2018 ; Menier et et al., 2017 ; Struth et al., 2020). Because a loss of drainage area is equivalent to a base-level rise (Willett et al., 2014), subsequent erosion of beheaded valleys is usually limited. Drainage beheading is also accompanied by reduced water and sediment discharge, such that it takes long, if ever, for this base-level rise to be compensated by sedimentary infill. As a consequence, beheaded valleys represent transient topographic states which can persist in the landscape over very long time periods (Jaiswara et al., 2019; Yang et al., 2015).

On the other hand, in building topographic barriers across pre-existing landscapes, displacement on dip-slip faults is an efficient driver of stream beheading (Burbank et al., 1996) (Fig. 1a). Beheaded streams can be used to quantify cumulative displacements on these faults (Moulin et al., 2016), determine the rate and sense of fault propagation (Kleber et al., 2021), and eventually constrain fault slip-rates when they contain datable material (Benedetti et al., 2000). Nevertheless, using these strain markers to reconstruct tectonic deformation is not straightforward. The reason for this is that they are restricted to only one fault compartment, and hence that their formation leaves no durable piercing-point at the surface of the opposite fault-block (Fig. 1a). This difficulty is usually tackled by modeling the pre-deformation profile as an extension of the still active upstream reach (Benedetti et al., 2000 ; Burbank et al., 1996 ; Jaiswara et al., 2019). This strategy is underlain by two main assumptions: (1) the pre-deformation profile was at steady-state at the time of beheading, and (2) the beheading event did not significantly modify the upstream profile. These assumptions, which are very difficult to test in practice, challenge the use of beheaded valleys as robust strain markers. For the same reason, their long theoretical lifetime remains little exploited, despite the fact that it offers an opportunity to quantify tectonic deformation over time-spans that are difficult to reach with other methods.

In this study, we propose a new approach, based on drainage-normalized stream profiles, which allows getting rid of assumption (1) provided that assumption (2) is true. This solution is expected to revive the use of beheaded valleys by morpho-tectonic studies, and stimulate the exploration of its potential for long-term tectonic reconstructions. We first describe the theory of the approach, and then present a method to apply it on natural prototypes using the Wadi-al-Akhdar graben in NW Saudi Arabia.

2. THEORY

Catchment loss quantification is best studied from χ-elevation plots (Struth et al., 2020; Whipple et al., 2017a). χ is a transformed stream channel coordinate, which describes the variation of drainage area in such a way that steady-state channels align along a straight line in the (χ-elevation) space (Perron and Royden, 2013):

$$\chi(x) = \int_{x_b}^{x} \left(\frac{A_0}{A(x)}\right)^{\frac{m}{n}} dx \quad \text{(Equation 1)}$$

where x is the distance along the stream channel, A(x) is the drainage area at distance x, x_b is the x-coordinate of the stream outlet, A_0 is a reference drainage area, and m/n is the concavity index (equation valid provided that the ratio of the tectonic uplift to the bedrock erodibility is invariant in the x dimension) assuming the streams follow a stream-power model (Whipple and Tucker, 1999).

When beheading occurs, the affected stream channel is instantaneously shifted far away from its steady-state (Willet et al., 2014). This is expressed in terms of χ as:

$$\chi(x) = \int_{x_b}^{x} \left(\frac{A_0}{A(x)-A_{lost}}\right)^{\frac{m}{n}} dx \quad \text{(Equation 2)}$$

where A_{lost} represents the lost catchment area, and A(x) represents the pre-beheading drainage area (same as in Equation 1). Modification of χ following a beheading event is thus sensitive to the ratio $A(x)/(A(x)-A_{lost})$ (Struth et al., 2020), which tends toward infinity when approaching the beheading point. As a result, χ-elevation plots of beheaded streams are pulled towards ever-increasing values of χ when moving upstream. Graphically, this translates into the well-known downward bending of the χ-elevation plot, hereafter referred to as "convex-up profiles" (dotted lines in Fig. 1b).

In terms of stream dynamics, a loss of drainage surface is equivalent to a base-level rise (Willett et al., 2014 ; Yang et al., 2015). A major implication is that the convex-up sections of χ-plot are prone to preservation over long time periods (Whipple et al., 2017b). This property implies that they broadly behave as structural datum that record vertical deformation, as long as they remain "below" the steady-state χ-elevation profile (Jaiswara et al., 2019 ; Whipple et al., 2017a). The (χ-elevation) encoding of tectonically beheaded streams is thus a combination of instantaneous downward bending and continuous tectonic warping (Fig. 1b).

Our objective is to extract the tectonic signal from this combined encoding. To do so, we focus on pairs of points located at the same distance from the fault but along two different downward branching beheaded channels (Fig. 1c). On the one hand, beheading causes the two points of each pair to be shifted differently in the χ dimension depending on their ratio $A(x)/(A(x)-A_{lost})$ (Struth et al., 2020) (Fig. 1b). On the other hand, their displacements in the vertical dimension are assumed to be consistent (i.e., the two points share the same post-beheading tectonic history: hereafter referred to as the "co-tectonic condition") (Fig. 1b). This latter assumption means that the method is applicable to channels that are geographically close to each other, and which have a beheading age difference that is small compared to the duration of the tectonic regime (in addition to the assumption that pre-beheading profiles are at steady-state).

Pairs of co-tectonic elements define co-tectonic lines (black lines in Fig. 1c and 1d) that rotate away from the steady-state elevation/χ slope as a function of their reconstructed ratio $A(x)/(A(x)-A_{lost})$. The key point here is that co-tectonic lines will become increasingly tangent to the steady-state profile as catchment loss corrections applied to χ approach the actual A_{lost} values (Fig. 1c and 1d). Therefore, a possible strategy to retrieve the initial unstrained geometry is to (1) explore the space of loss catchments solutions, (2) analyze the distribution of co-tectonic lines for each solution, and (3) evaluate its consistency with respect to steady-state conditions.

3. THE WADI AL-AKHDAR GRABEN : GEOMORPHIC SETTING OF THE NATURAL PROTOTYPE

We employed this approach using the Wadi al-Akhdar Graben (WAG, NW Saudi Arabia) as a case study. The WAG belongs to a series of narrow grabens that run sub-parallel to, and 200 km away from, the Northern Red Sea axis. The chronology of these grabens is poorly constrained. On the one hand, crustal extension associated to the opening of the Red Sea is considered to have concentrated near axis after 15Ma (Szymanski et al., 2016), suggesting these outboard structures have long been inactive. GPS velocities consistently suggest negligible present-day crustal deformation within the interiors of Saudi Arabia (Viltres et al., 2022). On the other hand, the spatial distribution of these grabens is closely associated to the Harrat

Uwayrid volcanic field (extending over the crest of highest elevation in the map of Fig. 2a), which has been (and perhaps still remains) active well beyond this chronologic limit (reported dates are as young as 340 ka ~ 50 km SW of the WAG: Altherr et al., 2019). This, as well as the occurrence of a sequence of shallow (3.2 km) earthquakes (M<=5.1) with NE-SW focal mechanisms about 20 km from the WAG (Xu et al., 2015), suggest that the upper crust of this area might continue to deform at small rates.

In any case, these grabens have a prominent geomorphic expression, marked by sharp normal fault escarpments and prominent evidence of drainage network disruption (Fig. 2). The WAG in particular consists of a 50-km-long 1-km-wide 100-150-m-deep depression bounded on either side normal fault scarps of up to ~ 100 m, and hosts intermittent water flow of the NW-flowing Wadi-al-Akhdar (Fig. 2). The geometry of the drainage basins on either side of the WAG clearly shows that displacement on the constitutive normal faults has sliced a pre-existing SW-NE-oriented stream network, and led to capture of the upstream catchments by the modern Wadi al-Akdhar (Fig. 2b and inset of Fig. 2a). Preservation of this geometry might result from the local climate aridity (annual rainfall of 80-100 m over the contributing catchments), which would have fossilized a >15-Ma-old stream network. Conversely, it might indicate that the WAG is much younger than 15Ma. Addressing this question is beyond the scope of the present study. The key point here is that the WAG constitutes an exceptionally well-preserved example of a tectonically beheaded stream network, with a series of wind-gaps preserved on the footwall of the NE border fault (Fig. 2b).

Quantification of post-beheading tectonic deformation using the traditional method (i.e., across-fault extrapolation of the still active upstream channel profile) yields vertical displacement around 55 m for about 3-4 km from the fault (Fig. 3). How would this estimate get modified by employing the strategy described in the previous section ?

To answer that question, we focused on the pair of beheaded valleys (labelled V1 and V2 in Fig. 2b) that are the most unequivocally interpreted in terms of catchment area loss. These two streams are ~1.6 km apart at their intersection with the escarpment of the NE border fault, and branch downstream at ~3 km from the fault. At distances >1km from the fault, the valley floors are 40-m-wide in average and entrenched by ~40-60 m within the massive sandstone beds of the Tabuk Formation (Geologic Map of the Shaghab Quadrangle, Sheet 27B, Kingdom of Saudi Arabia). The valley morphology changes when approaching the tectonic escarpment. At about 1 km from the fault, V1 becomes wider (up to ~100 m) and flatter in cross-section, and fine-grained sediments become abundant on the valley floor. Farther upstream, a reversal of the valley slope is observed at about 500 m from the fault, and marks the regressive erosion of a short stream channeled to the base of the NE border fault (Fig. 2b). Similar enlargement and infill by fine-grained sediments are observed along V2 at less than ~1km from the fault, but there is no evidence of slope reversal or regressive erosion. These distinctive characters occur in the very upper part of the modern catchments (~1km^2), where it is well known that the morphology is largely controlled by hillslope processes (Struth et al., 2020). These valley sections will thus be ignored in the following analysis. Looking at the upstream catchments, it seems obvious that V1 used to drain catchment A, whereas V2 was the downstream reach of catchment B (Fig. 2b ; see also inset of Fig. 2a).

4. RESULTS

Drainage area and χ have been computed from a 2-m-resolution DEM constructed from stereo SPOT6 satellite imagery (see Supporting Information Text S1) and using the TopoToolBox functions (Schwanghart et al., 2014). χ was calculated using typical values of 0.45 for the concavity index and 1km^2 for A_0 (Equations 1 and 2). We focused on the system composed by V1 and V2 and the main trunk below their confluence. The χ-elevation plot reveals a downstream section which is very slightly convex upward, and a

steepened upstream section that extends from ~600m upstream from the confluence up to the end of the profile (Fig. 4). Clearly, the convex-up morphology expected from the loss of drainage area is at least not obvious, which indicates that they also contain a vertical deformation signal.

Our analysis assumes that the stream profiles just before beheading were at steady-state and in equilibrium with a spatially invariant ratio of the tectonic uplift to the bedrock erodibility (i.e., the chi-plots were initially straight: see Fig. 1b). This assumption implies that the time interval separating the onset of faulting from the beheading event was short enough for the pre-beheading stream profiles to remain essentially controlled by the pre-faulting forcing (i.e., uplift-rate equal to zero or to any other spatially invariant value at the scale of the analyzed drainages). The impact of this assumption is discussed in the last section of the article.

We have explored the space of catchment loss solutions by varying two parameters. On one hand, the total lost area (streams 1+2) was varied from 0 to 300km^2 (i.e., approximately twice the value estimated from the observed basin geometries; see inset of Fig. 2a) using increments of 15km^2. On the other hand, the proportion of this total lost area ascribed to V1 was varied between 0 to 1 using increments of 0.05. For each scenario, the co-tectonic lines have been computed by interpolating χ and elevation along streams 1 and 2 at regularly spaced distances (2m) from the fault, and determining their gradient and intercept from the χ-elevation pair of even fault-distance points.

In a first step, the solution space can be reduced by analyzing the sign of slope of the co-tectonic lines, as these lines must by definition slope downstream (positive sign). Our simulation shows that the co-tectonic lines slope upstream for a V1 catchment loss proportion lower than 0.5 (i.e., negative sign: see inset of Fig. 5). There is an evident reason for this: since our approach assumes that tectonic deformation does not vary from V1 to V2, the higher position of V2 relative to V1 in the χ-elevation necessarily requires V1 proportion to be higher than V2 proportion.

For each solution, we have then analyzed the distribution of the co-tectonic lines relative to the downstream section of the corrected profile. To do so, we have selected a reference point of the main trunk sufficiently far away from the fault to ensure it is not affected by faulting-related uplift. The narrowness of the WAG (Fig. 2a) indicates that it is a shallow structure propagating no more than a few kilometers deep. On the other hand, normal-faulting-controlled uplift extends to distances that scale with the thickness of crust involved in the deformation (Armijo et al., 1996). We thus considered a distance of 10 km as a safe buffer for the WAG, and picked the reference point at that distance (red point in the inset of Fig. 4).

We recall that co-tectonic lines should become increasingly tangent to the steady-state profile (see Theory), and hence distribute just above the reference point, as catchment loss corrections approach the actual values (Fig. 1c and 1d). The best solution is thus estimated by computing the elevation of individual co-tectonic lines at the reference χ (hereafter referred to as "projected elevation"), and analyzing their distribution relative to the reference elevation. The results show little sensitivity to the total lost area (Fig. 5), but do show a convergence regarding the relative proportion of lost areas. The best fit is obtained for a V1 proportion of ~0.8. This value is very close to that determined from the geometry of the upstream basins (i.e., ~0.84 ; see inset of Fig. 2a), which therefore supports the use of our approach.

The cumulative uplift recorded by the 2 valleys can then be readily quantified by propagating the mean slope of the co-tectonic lines from the reference point (Fig. 6). The obtained uplift profiles depend on the total lost area (Fig. 6), a parameter that we cannot resolve precisely with our method. However, the dispersion remains small except for scenario where the lost area is extremely small (i.e., < 20% of the observed value) (Fig. 6).

5. DISCUSSION AND CONCLUSION

The very good match between the proportion of catchment loss obtained from our approach when applied to WAG and that measured from the actual upstream drainage, indicates that the long profiles of V1 and V2 have been essentially preserved since the beheading event. This in turn supports the view that a loss of drainage area results in the preservation of transient states in the landscape (Whipple et al., 2017b), although it is likely favored by the local climate aridity in the case of the WAG. On the other hand, our approach is not very effective to quantify the total catchment loss (Fig. 5), which in turn results in uncertainties regarding the magnitude of uplift (Fig. 6). However, large uncertainties exist only for extreme values of catchment loss (< 20% of the actual value). This indicates that loose constraints on catchment area loss (obtained for example from the dimension of the beheaded valleys) might be sufficient to quantify tectonic uplift with reasonable uncertainties.

The new approach developed in the present article to quantify the cumulative uplift recorded by tectonically beheaded valleys assumes steady-state profiles at the time of catchment loss. It is worth noting that this assumption has distinct implications depending on the chronology of events. For one end-member, beheading is synchronous with the onset of faulting, which means that the pre-beheading profiles are in equilibrium with a spatially constant uplift-rate equal to zero (or any other value), and are thus characterized by a linear chi-plot (equivalent to the black line in Fig. 1b). For the other end-member, beheading occurs sufficiently long after the onset of faulting for the stream profiles to be in equilibrium with a spatially variable uplift-rate at the time of beheading. In this latter case, the chi-plot must have a concave-up shape which mirror the uplift profile of Fig. 1a (Perron and Royden, 2013). Both the traditional method and the new approach described in this article implicitly assume the first end-member. Although our results seem to indicate that this assumption is valid in the case of the WAG, it likely does not hold in general.

If the second end-member applies, then the way we estimate the preferred solution from the distribution of co-tectonic lines would not work, because the chi-plots immediately before beheading would not form a straight line. However, the co-tectonic lines formulation offers an avenue to treat that case. We describe here a possible strategy based on the example of Fig. 1, but assuming the second end-member. Just before beheading, the slope of the chi-plot would decrease away from the fault along with the decrease of the uplift-rate (Fig. 1a), instead of forming a straight line as in Fig. 1b. In addition, the slope would become constant beyond the edge of the deforming zone (at distance lower than ~ 18 km in Fig. 1a). Because each co-tectonic line represents the slope of the pre-beheading chi-plot at a given distance from the fault (and hence for a given uplift-rate), they are expected to follow the same pattern (i.e., display slopes that decrease away from the fault and stabilize beyond the edge of the deforming zone). Examining the progressive stabilization of the co-tectonic line slopes away from the fault thus represents a possible way to deal with initially non-linear chi-plots. This should be a topic of future extension of our method to other natural prototypes.

Beside this perspective, the main advance provided by our approach is that it does not use any information from the lost catchments upstream from the fault. Whereas the change in base-level that necessarily accompanies the capture of these catchments can greatly affect the results of the traditional method, it has no effect on the approach presented here (compare Fig. 3 with Fig. 6). This also implies that this approach becomes increasingly useful as ambiguities about the pre-deformation drainage topology becomes significant. This advantage should become all the more decisive when attempting to reconstruct tectonic deformation accumulated over long time periods (Moulin et al., 2016). We believe that, once calibrated against other field examples, our approach could allow quantifying tectonic deformation over timescales that are difficult to access with current methods (i.e., several hundreds of ka or more).

ACKNOWLEDGMENTS

This research was supported by King Abdullah University of Science and Technology (KAUST) under the Award Number OSR-CRG2019-4076.

OPEN RESEARCH

The 2m DEM derived from Pleiades images photogrammetry as well as the code developed through this study can be requested to the corresponding author.

REFERENCES

Altherr, Rainer, Regina Mertz-Kraus, Frank Volker, Hans Kreuzer, Friedhelm Henjes-Kunst, and Ulrich Lange. "Geodynamic setting of Upper Miocene to Quaternary alkaline basalts from Harrat al 'Uwayrid (NW Saudi Arabia): Constraints from KAr dating, chemical and Sr-Nd-Pb isotope compositions, and petrological modeling." *Lithos* 330 (2019): 120-138.

Armijo, Rolando, B. G. C. P. Meyer, G. C. P. King, Alexis Rigo, and D. Papanastassiou. "Quaternary evolution of the Corinth Rift and its implications for the Late Cenozoic evolution of the Aegean." *Geophysical Journal International* 126, no. 1 (1996): 11-53.

Benedetti, Lucilla, Paul Tapponnier, Geoffrey CP King, Bertrand Meyer, and Isabelle Manighetti. "Growth folding and active thrusting in the Montello region, Veneto, northern Italy." *Journal of Geophysical Research: Solid Earth* 105, no. B1 (2000): 739-766.

Bonnet, Stephane. "Shrinking and splitting of drainage basins in orogenic landscapes from the migration of the main drainage divide." *Nature Geoscience* 2, no. 11 (2009): 766-771.

Burbank, Douglas, Andrew Meigs, and Nicholas Brozović. "Interactions of growing folds and coeval depositional systems." *Basin research* 8, no. 3 (1996): 199-223.

Giachetta, Emanuele, and Sean D. Willett. "Effects of river capture and sediment flux on the evolution of plateaus: insights from numerical modeling and river profile analysis in the upper Blue Nile catchment." *Journal of Geophysical Research: Earth Surface* 123, no. 6 (2018): 1187-1217.

Jaiswara, Nilesh Kumar, Prabha Pandey, and Anand K. Pandey. "Mio-Pliocene piracy, relict landscape and drainage reorganization in the Namcha Barwa syntaxis zone of eastern Himalaya." *Scientific reports* 9, no. 1 (2019): 17585.

Kleber, Emily J., Duane E. DeVecchio, J. Ramón Arrowsmith, and Tammy M. Rittenour. "Spatiotemporal Rates of Tectonic Deformation and Landscape Evolution above a Laterally Propagating Thrust Fault: Wheeler Ridge Anticline, California, USA." *Lithosphere* 2021, no. Special 2 (2021): 3395719.

Menier, David, Manoj Mathew, Manuel Pubellier, François Sapin, Bernard Delcaillau, Numair Siddiqui, Mu Ramkumar, and M. Santosh. "Landscape response to progressive tectonic and climatic forcing in NW Borneo: Implications for geological and geomorphic controls on flood hazard." *Scientific Reports*7, no. 1 (2017): 457.

Moulin, Adrien, Lucilla Benedetti, Magali Rizza, Petra Jamšek Rupnik, Andrej Gosar, Didier Bourles, Karim Keddadouche et al. "The Dinaric fault system: Large-scale structure, rates of slip, and Plio-Pleistocene evolution of the transpressive northeastern boundary of the Adria microplate." *Tectonics* 35, no. 10 (2016): 2258-2292.

Perron, J. Taylor, and Leigh Royden. "An integral approach to bedrock river profile analysis." *Earth surface processes and landforms* 38, no. 6 (2013): 570-576.

Schwanghart, Wolfgang, and Dirk Scherler. "TopoToolbox 2–MATLAB-based software for topographic analysis and modeling in Earth surface sciences." *Earth Surface Dynamics*2, no. 1 (2014): 1-7.

Struth, Lucía, Emanuele Giachetta, Sean D. Willett, Lewis A. Owen, and Eliseo Tesón. "Quaternary drainage network reorganization in the Colombian Eastern Cordillera plateau." *Earth Surface Processes and Landforms* 45, no. 8 (2020): 1789-1804.

Szymanski, E., D. F. Stockli, P. R. Johnson, and C. Hager. "Thermochronometric evidence for diffuse extension and two-phase rifting within the Central Arabian Margin of the Red Sea Rift." *Tectonics* 35, no. 12 (2016): 2863-2895.

Viltres, Renier, Sigurjón Jónsson, Abdulaziz O. Alothman, Shaozhuo Liu, Sylvie Leroy, Frédéric Masson, Cécile Doubre, and Robert Reilinger. "Present-Day Motion of the Arabian Plate." *Tectonics* 41, no. 3 (2022): e2021TC007013.

Whipple, K. X., A. M. Forte, R. A. DiBiase, N. M. Gasparini, and W. B. Ouimet. "Timescales of landscape response to divide migration and drainage capture: Implications for the role of divide mobility in landscape evolution." *Journal of Geophysical Research: Earth Surface* 122, no. 1 (2017): 248-273.

Whipple, Kelin X., Roman A. DiBiase, William B. Ouimet, and Adam M. Forte. "Preservation or piracy: Diagnosing low-relief, high-elevation surface formation mechanisms." *Geology* 45, no. 1 (2017): 91-94.

Whipple, Kelin X., and Gregory E. Tucker. "Dynamics of the stream-power river incision model: Implications for height limits of mountain ranges, landscape response timescales, and research needs." *Journal of Geophysical Research: Solid Earth* 104, no. B8 (1999): 17661-17674.

Willett, Sean D., Scott W. McCoy, J. Taylor Perron, Liran Goren, and Chia-Yu Chen. "Dynamic reorganization of river basins." *Science* 343, no. 6175 (2014): 1248765.

Xu, Wenbin, Rishabh Dutta, and Sigurjón Jónsson. "Identifying active faults by improving earthquake locations with InSAR data and Bayesian estimation: the 2004 Tabuk (Saudi Arabia) earthquake sequence." *Bulletin of the Seismological Society of America* 105, no. 2A (2015): 765-775.

Yang, Rong, Sean D. Willett, and Liran Goren. "In situ low-relief landscape formation as a result of river network disruption." *Nature* 520, no. 7548 (2015): 526-529.

FIGURE CAPTIONS

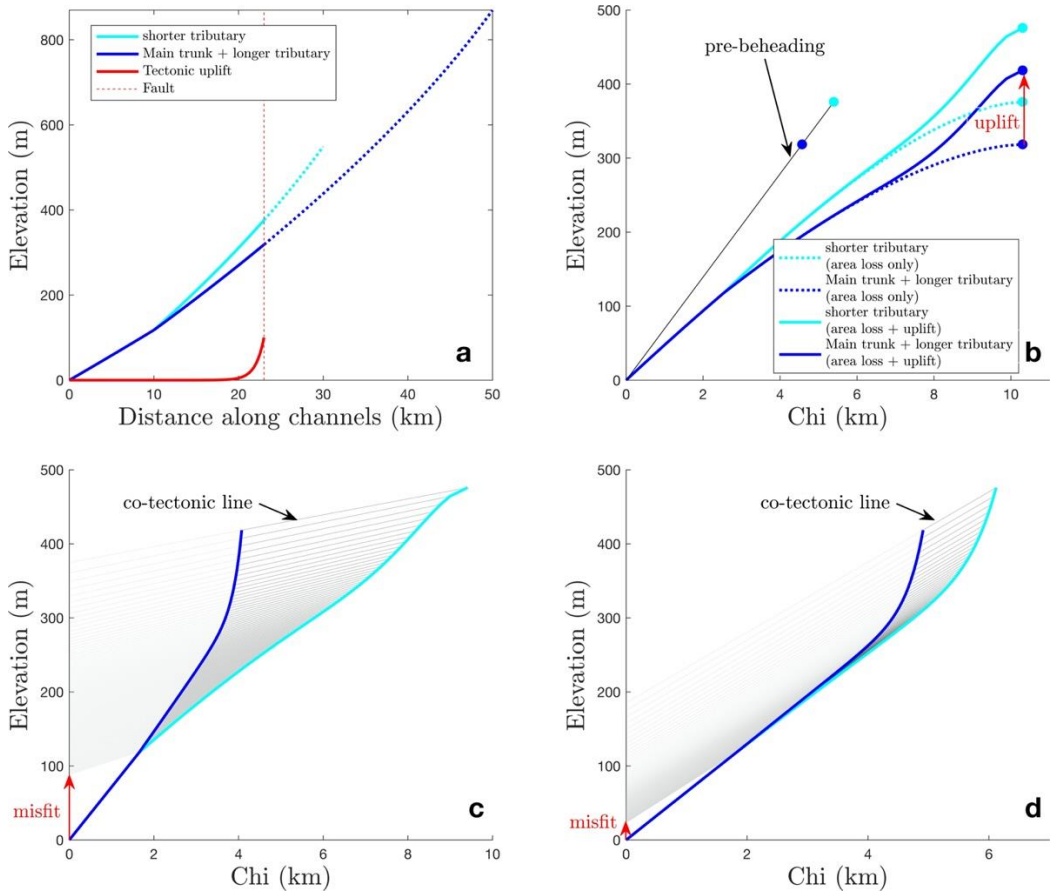

Figure 1: Synthetic stream profiles that illustrate the approach employed to quantify the uplift recorded by tectonically beheaded valleys. (a) The long profile of a main trunk and its two tributaries, and the total uplift profile caused by slip on a normal fault are plotted against distance along channel. Streams are assumed to obey the stream-power model (Whipple and Tucker, 1999) and be at equilibrium at the time of beheading.

The dotted stream sections are those lost by tectonic beheading. (b) Chi-plots of the same streams after beheading. Only the stream sections downstream from the fault are represented. Note how the "convex-up" signal caused by drained area loss is obscured by subsequent tectonic uplift. The circles depict the intersection between the tributaries and the fault, just before beheading, just after beheading, and after the accumulation of tectonic uplift. (c and d) Two corrected chi-plots are represented by assuming different values of lost areas for the two tributaries. The co-tectonic lines rotate depending on the assumed values, and their distribution becomes increasingly tangent to the downstream not uplifted section as the assumed values approach the actual one (i.e., when moving from c to d).

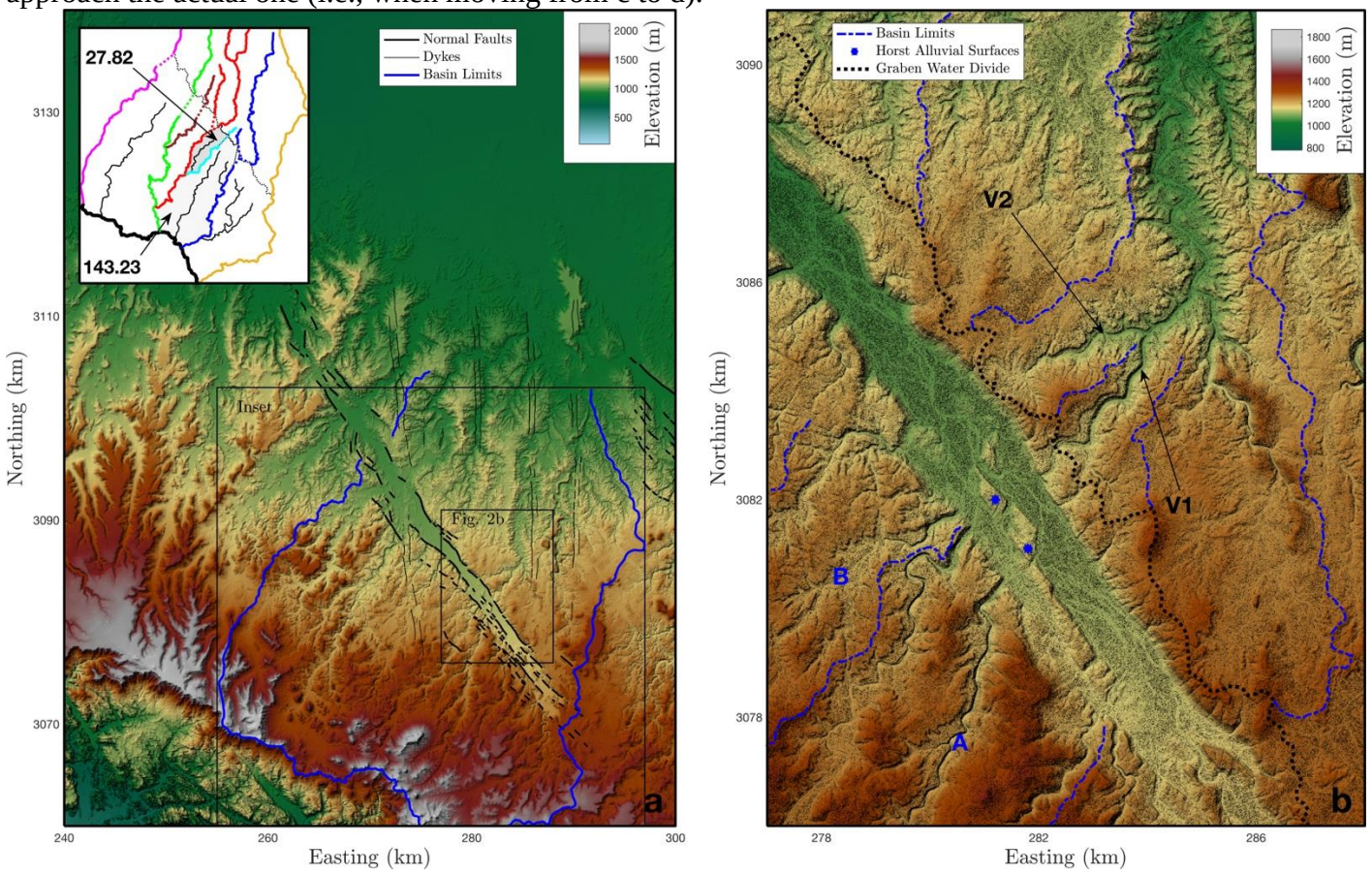

Figure 2: Topographic maps above the stream network beheaded by cumulative displacement on the normal fault of the Wadi-al-Akhdar Graben. (a) Large scale map (30m TanDEM-X) showing the relation between normal faulting (mapped from DEM analysis and field observations) and drainage geometry. The SW-facing escarpment in the lower left corner of the map is the NE edge of the Red Sea Rift. The inset shows the across-WAG correlation of catchment limits within the area delineated with a blue line in the main figure (black catchment limits have no equivalent on the NE side of the graben). The values in the inset depict the lost catchment surface (in km^2) of valleys V1 and V2 shown in (b). (b) Closer view of the intersection of valleys V1 and V2 with the WAG (2-m-resolution DEM derived from photogrammetry of stereo Pleiades images). A and B represent the interpreted lost catchments of V1 and V2. The black dashed line depicts the water-divide of the graben.

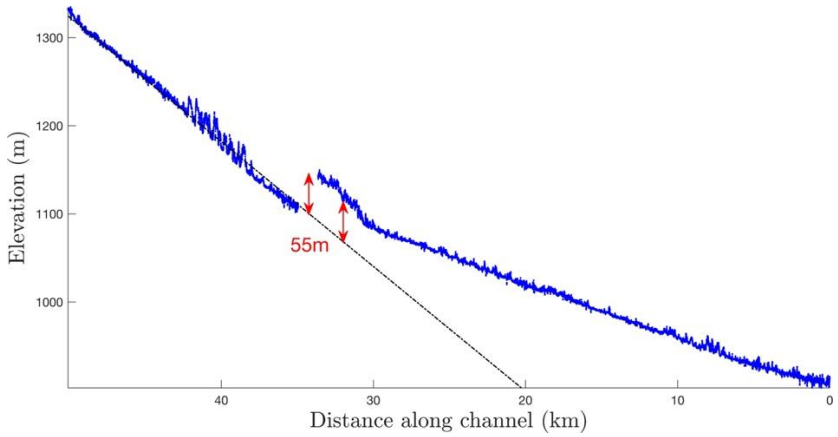

Figure 3: Longitudinal profiles of the main stream of catchment A and of V1 on both sides of the WAG. The dashed line represents the initial undeformed profile that would be estimated from the upstream still active section to determine the tectonic uplift recorded by V1. Comparison with Figure 6 shows how this estimation would bias both the magnitude and distribution of the calculated uplift.

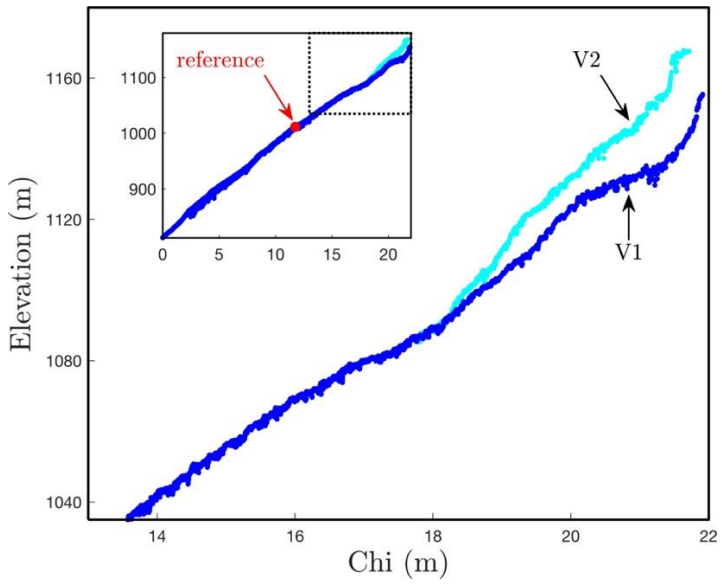

Figure 4: Chi-plots of V1, V2, and their downstream trunk computed from a 2-m-resolution DEM, and using a concavity index (m/n in Equations 1 and 2) of 0.45. Note the absence of a clear "convex-up" signal that would be expected from the catchment loss. The inset shows the same chi-plots extending downstream, with the extent of the main figure shown with a dotted box.

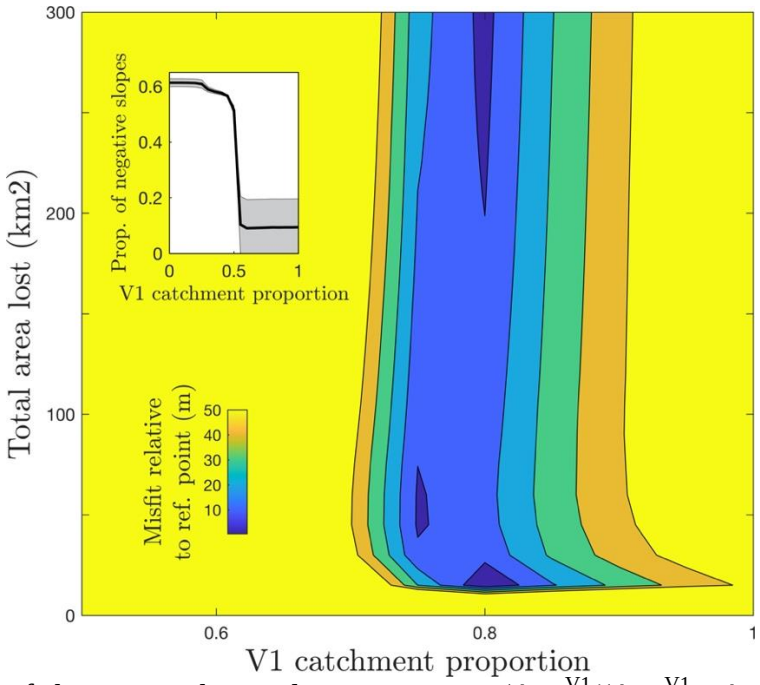

Figure 5: Determination of the V1 catchment loss proportion ($A_{lost}^{V1}/(A_{lost}^{V1}+ A_{lost}^{V2})$) using the approach depicted in Figures 1c and 1d. The "misfit relative to reference point" is equivalent to the red arrow shown in Figures 1c and 1d. The inset shows the proportion of negative co-tectonic slopes obtained from the analysis as a function of V1 catchment loss proportion, and indicates that proportions lower than 0.5 are not permitted.

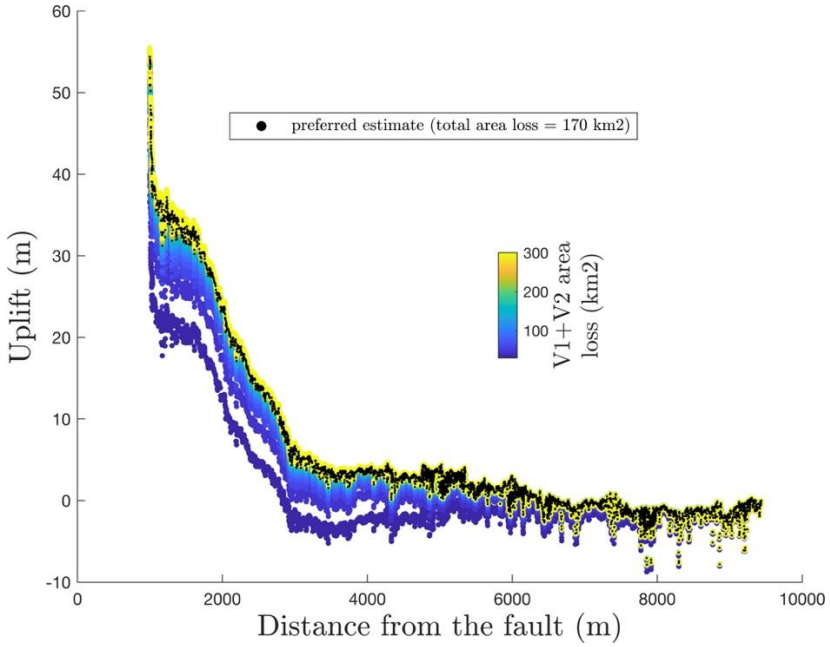

Figure 6: Tectonic uplift recorded by V1 and V2 for a range of total loss solutions. All these solutions conform with a V1/(V1+V2) catchment loss proportion of 0.8 as determined from Figure 5. The preferred estimate comes from the two solutions of lowest misfit (Figure 5), which also have a total loss value close to that determined from the actual catchment geometries (inset of Figure 1a).